LANGMUIR

pubs.acs.org/Langmuir Article

Dynamic Effects during the Capillary Rise of Fluids in Cylindrical Tubes

Stephan B. Lunowa,* Arjen Mascini, Carina Bringedal, Tom Bultreys, Veerle Cnudde, and Iuliu Sorin Pop

Cite This: *Langmuir* 2022, 38, 1680−1688 Read Online

ACCESS | Metrics & More | Article Recommendations | Supporting Information

ABSTRACT: The mathematical models for the capillary-driven flow of fluids in tubes typically assume a static contact angle at the fluid−air contact line on the tube walls. However, the dynamic evolution of the fluid−air interface is an important feature during capillary rise. Furthermore, inertial effects are relevant at early times and may lead to oscillations. To incorporate and quantify the different effects, a fundamental description of the physical processes within the tube is used to derive an upscaled model of capillary-driven flow in circular cylindrical tubes. The upscaled model extends the classical Lucas−Washburn model by incorporating a dynamic contact angle and slip. It is then further extended to account for inertial effects. Finally, the solutions of the different models are compared to experimental data. In contrast to the Lucas−Washburn model, the models with dynamic contact angle match well the experimental data, both the rise height and the contact angle, even at early times. The models have a free parameter through the dynamic contact angle description, which is fitted using the experimental data. The findings here suggest that this parameter depends only on the properties of the fluid but is independent of geometrical features, such as the tube radius. Therefore, the presented models can predict the capillary-driven flow in tubular systems upon knowledge of the underlying dynamic contact-angle relation.

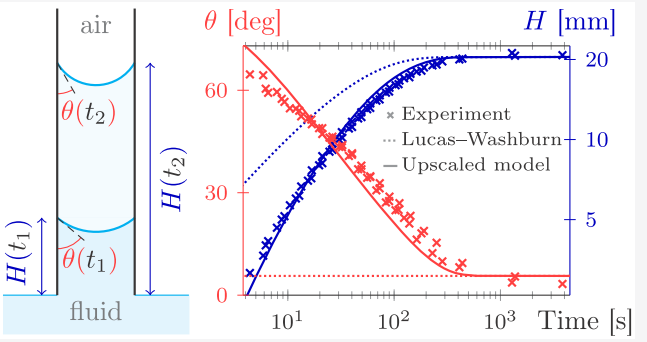

INTRODUCTION

One hundred years ago, the classical works of Lucas,[1] Washburn,[2] Rideal,[3] and Bosanquet[4] laid the foundation for the description of the capillary-driven flow of fluids in porous structures. Since then, this field of research has gained attention because of its various applications, ranging from water transport in soil and plants, over printing with ink, to oil recovery and CO_2 sequestration. To understand the flow processes in a porous medium, knowledge about the fluid dynamics within its fundamental structures, the single pores, is needed. In these, the surface tension leads to capillary-driven flow. An overview on the topic can be found in the recent review by Cai et al.[5]

The model of Lucas and Washburn describes the balance between capillary and hydrostatic pressure, leading to viscous flow until equilibrium at the so-called Jurin's height is reached. Fries and Dreyer[6] derived a formulation for the solution of the Lucas−Washburn equation that remains valid also at late times. Levine et al.[7] studied in detail the resulting flow close to the fluid−air interface, assuming a spherical meniscus and low Reynolds numbers. Although these basic mechanisms are well-understood, the complex wetting effects lead to a dynamic evolution of the interface, in particular of both its shape and position. An important feature is the contact angle formed between the fluid−air interface and the pore wall. In the aforementioned works, this contact angle is assumed constant. However, experimental results invalidate this assumption, in particular at early times.[8,9] Martic et al.[10,11] discussed this based on molecular dynamics simulations and the molecular kinetics theory. This theory is also used by Hamraoui and Nylander[12] to discuss the effect of a dynamic contact angle as a source of interface retardation and viscous dissipation. Chebbi[13] and Popescu et al.[14] compare several dynamic contact-angle models when applied to the Lucas−Washburn equation.

Furthermore, inertial effects are relevant for early times of capillary rise, as discussed in detail by Quéré,[15] and for low viscous fluids they can even lead to (damped) oscillations around Jurin's height at late times. Xiao et al.[16] additionally considered the end effect at the reservoir (sink flow) for parallel plates and tubes and derived a double Dirichlet series

Received: October 8, 2021
Revised: January 14, 2022
Published: January 25, 2022

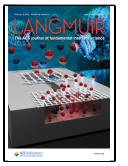

https://doi.org/10.1021/acs.langmuir.1c02680
Langmuir 2022, 38, 1680−1688

representation of the solution. An overview of the different regimes has been given by Zhmud et al.[17] as well as by Fries and Dreyer.[18] However, all these models are based on the assumption of a static contact angle.

To incorporate and quantify the influence of the different effects of the dynamic contact angle and of inertia, one should start with a derivation based on the fundamental description within the tube. Considering this detailed pore-scale model, and under suitable assumptions on the nondimensional parameters like the Reynolds and capillary number, one can employ asymptotic expansion techniques to derive an effective, so-called upscaled model for the relevant quantities like flux, pressure, and rise height. The result is an upscaled model that describes the effective behavior of the relevant physical quantities, which can be validated using experimental data. Thereby, the dynamics of the capillary rise including the detailed evolution of the contact angle becomes predictable. Furthermore, the application of these extended models helps to reduce the observed discrepancy[9] between the experiments and the classical Lucas–Washburn model.

In this paper, the upscaling of the capillary-driven flow in cylindrical tubes is discussed first. The result is an upscaled model, which is a nonlinear first-order differential equation of the Lucas–Washburn type. This is solved analytically to obtain directly usable solutions. While capillary-rise models with dynamic contact angle have been described in the literature, to the best of the authors' knowledge, this work is the first to derive such a model rigorously by upscaling. The upscaled model is then extended to incorporate inertial effects. To validate the theory, the solutions to the upscaled and to the extended model are compared to the experimental results reported by Heshmati and Piri.[9] This includes the simultaneous comparison to the provided height and contact-angle data for different fluids and several radii, which has not been presented before. Finally, the results of the comparison including uncertainties and limitations are discussed. More details of the upscaling procedure and of the comparison are presented in the Supporting Information.

MATERIALS AND METHODS

First, the derivation of the upscaled model and its analytical solution are discussed. To this end, the capillary-driven flow in circular cylindrical tubes is modeled by the Navier–Stokes equations. These equations are defined in an evolving domain, as the fluid–air interface is moving because of capillary effects. The model includes a dynamic contact angle and slip. Then, a matched asymptotic expansion method is applied to obtain the effective model. Thereafter, the model is extended to incorporate inertial effects.

Upscaled Model and Analytic Solution. In the following, we summarize the derivation of the upscaled model based on the ideas presented by Lunowa et al.[19] The detailed derivation of the equation is provided in the Supporting Information, where the details and assumptions for the nondimensionalization and the asymptotic expansion are given.

The flow of a fluid in a thin, vertical tube, driven by the surface tension at the fluid–air interface, can be modeled by the Navier–Stokes equations defined in a time-dependent domain, where the fluid–air interface is a free boundary. Assuming a small Reynolds number, one can derive the solution by a matched asymptotic expansion for the limit of a vanishing radius-to-length ratio $\varepsilon = R/L \ll 1$ (R being the tube radius and L Jurin's height). The result is Hagen–Poiseuille flow driven by the difference between the surface tension and the hydrostatic pressure. In the dimensionless form, the evolution of the fluid rise height h is then governed by

$$p_{\mathrm{in}} - h - \frac{8h}{1+4\lambda}\frac{\mathrm{d}h}{\mathrm{d}t} = -\frac{2\cos\left[\theta\left(\frac{\mathrm{d}h}{\mathrm{d}t}\right)\right]}{\mathrm{Ca}} \tag{1}$$

Here p_{in} is the pressure at the inlet (bottom), λ denotes the slip length at the tube wall, and Ca is the capillary number (see Figure 1). Note

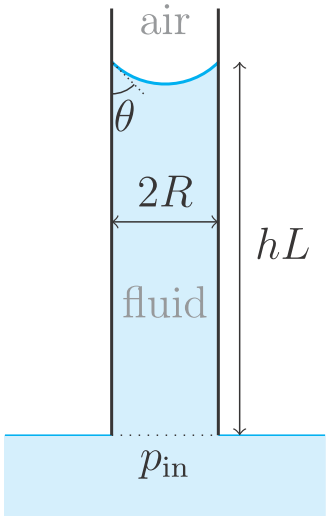

Figure 1. Schematic drawing of the tube with radius R. The contact angle θ is formed between the tube wall and the fluid–air interface at rise height hL. The inlet pressure p_{in} is attained between tube and reservoir.

that the dynamic contact angle θ may depend on the velocity of the interface. Furthermore, eq 1 resembles the relation derived by Washburn,[2] based on macroscopic arguments. However, Washburn discussed only the case of a static contact angle, whereas here a dynamic contact-angle model is incorporated.

In the context of capillary rise experiments, the pressure at the inlet is approximately atmospheric, i.e., $p_{\mathrm{in}} = 0$. The typical length scale is given by the equilibrium or Jurin's height $L = 2\sigma\cos(\theta_s)/(\rho g R)$, attained as $t \to \infty$, and which is depending on the fluid–air surface tension σ, the static contact angle θ_s (measured in the fluid), the density ρ of the fluid, the gravitational acceleration $g = 9.81\ \mathrm{m/s^2}$, and the tube radius R. This yields $\mathrm{Ca} = 2\cos(\theta_s)$ (cf. the Supporting Information), so that eq 1 becomes

$$\frac{8h}{1+4\lambda}\frac{\mathrm{d}h}{\mathrm{d}t} = \frac{\cos\left[\theta\left(\frac{\mathrm{d}h}{\mathrm{d}t}\right)\right]}{\cos(\theta_s)} - h \tag{2}$$

for all $t > 0$. Clearly, the solution $h = h(t)$ depends on the contact-angle model. However, the specific choice of this model is uncertain without much reference data, because the differences resulting after fitting the different models are typically very small.[14,20] For simplicity, a linear model in the velocity is considered here, which was also used frequently as a simplification of the molecular kinetics theory,[10−12,14,20−22] valid at low velocities. Specifically,

$$\cos(\theta(v)) = \cos(\theta_s) - \eta\,\mathrm{Ca}\,v$$

where the dynamic parameter $\eta \geq 0$ denotes the strength of the linear response due to the interface velocity $v = \frac{\mathrm{d}h}{\mathrm{d}t}$. Note that this model arises naturally for all possible contact-angle models after linearization using the relation $\cos\tilde{\theta}(v) \approx \cos\tilde{\theta}(0) - \sin\tilde{\theta}(0)\frac{\mathrm{d}\tilde{\theta}}{\mathrm{d}v}(0)v$ and therefore is generic. Other models could be used as well; however, the advantage of the linear model is that the resulting equation can be solved analytically, as discussed in the following. With this contact-angle model, the rise model eq 2 becomes

https://doi.org/10.1021/acs.langmuir.1c02680
Langmuir 2022, 38, 1680−1688

$$\left(\frac{8h}{1+4\lambda}+2\eta\right)\frac{\mathrm{d}h}{\mathrm{d}t}=1-h \tag{3}$$

for all $t > 0$. A natural initial condition is

$$h(0)=0 \tag{4}$$

Observe that, because 1 is an equilibrium solution to eq 3, the solution to the initial value problem (eqs 3 and 4) remains below 1 for all times t. Moreover, h is increasing. By separation of variables, the solution to eqs 3 and 4 is obtained in implicit form

$$(1-h(t))\exp\left(\frac{4h(t)}{(1+4\lambda)\eta+4}\right)=\exp\left(-\frac{(1+4\lambda)t}{2(1+4\lambda)\eta+8}\right) \tag{5}$$

Because h is monotonic, using eq 5 one can express t as a function of h, namely

$$t=t(h)=-\frac{8h}{1+4\lambda}-\frac{2(1+4\lambda)\eta+8}{1+4\lambda}\ln(1-h)$$

At early times, this yields

$$t\approx 2\eta h+\left(\eta+\frac{4}{1+4\lambda}\right)h^2$$

If $\eta = 0$, this resembles the classical Lucas–Washburn equation. If $\eta > 0$, the first term implies a linear time–height relation at early times, when $h \ll 1$, and therefore, quadratic terms can be neglected. Figure 2 illustrates possible solutions. The dynamic parameter η determines the velocity of the rise in the beginning, because eq 3 yields $\frac{\mathrm{d}h}{\mathrm{d}t}(0)=\frac{1}{2\eta}$. In particular, it is singular if $\eta = 0$, because inertial terms and the movement of the air are neglected. On the other hand, the influence of the slip length λ on the velocity increases with increasing height h. Furthermore, for $\eta > 0$, this yields an initial contact angle $\theta = 90°$ at time $t = 0$.

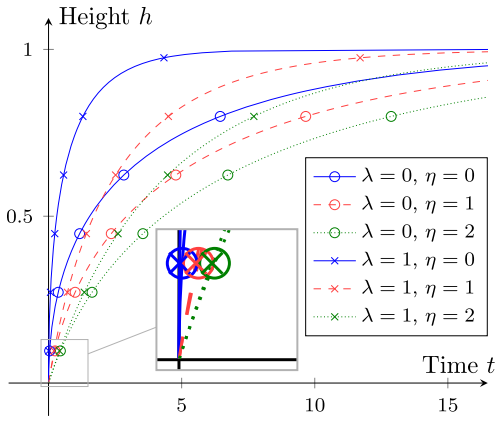

Figure 2. Height of the capillary rise given by eq 5 increases faster for higher slip length λ. The dynamic parameter η retards the rise and determines the initial velocity at time $t = 0$.

Extended Model Including Inertial Effects. The upscaled model described above requires the Reynolds number to be small. In the case of a low viscosity, or when the tube radius increases, the Reynolds number becomes large, so that one cannot neglect inertial effects. In that situation, the upscaling procedure does not yield a closed expression for the height of the capillary rise, as the system remains fully coupled. Instead, an empirical extension of the upscaled model is used, based on macroscopic considerations.[4,12,17,18,22] In these references, the balance between hydrostatic, inertial and capillary forces was considered assuming Hagen–Poiseuille flow and a spherical meniscus. In this context, the resulting balance reads

$$\mathcal{I}\frac{\mathrm{d}}{\mathrm{d}t}\left(h\frac{\mathrm{d}h}{\mathrm{d}t}\right)+\left(\frac{8h}{1+4\lambda}+2\eta\right)\frac{\mathrm{d}h}{\mathrm{d}t}=1-h \tag{6}$$

where $\mathcal{I}=\varepsilon^2\mathrm{Re}=\rho^3 g^2 R^5/(2\mu^2\sigma\cos(\theta_s))$ is the inertial coefficient (see the Supporting Information). Note that the denominator $(1 + 4\lambda)$ accounts for slip, and the term $2\eta\frac{\mathrm{d}h}{\mathrm{d}t}$ is due to the linearized contact-angle model. Note that this extended model (eq 6) is closely related to the modified Lucas–Washburn equation discussed by Martic et al.[10,11] However, they considered a model that does not account for a slip length λ.

With eq 4, this nonlinear second-order differential equation (eq 6) becomes degenerate. Furthermore, one needs to specify a second initial condition, similar to the initial velocity. For this purpose, one can use an asymptotic analysis carried out for $t \to 0$ with ansatz $h(t) = ct^\alpha + o(t^\alpha)$.[17,22] Equating the leading order terms yields $h(t) \sim t/(\eta + \sqrt{\eta^2 + \mathcal{I}})$, and hence

$$\left.\frac{\mathrm{d}h}{\mathrm{d}t}\right|_{t=0}=\frac{1}{\eta+\sqrt{\eta^2+\mathcal{I}}} \tag{7}$$

To solve the initial value problem (eqs 4, 6, and 7) numerically, it is reformulated as a system of nonlinear first-order differential equations in the variables $w := h^2$ and $v := \frac{\mathrm{d}w}{\mathrm{d}t}$. Equation 6 then becomes

$$\frac{\mathrm{d}w}{\mathrm{d}t}=v,\qquad \frac{\mathrm{d}v}{\mathrm{d}t}=\frac{2}{\mathcal{I}}\left(1-\sqrt{w}-\left(\frac{4}{1+4\lambda}+\frac{\eta}{\sqrt{w}}\right)v\right)$$

To avoid the singularity at $w = 0$, the initial conditions used here are $w(0) = 10^{-12}$ and $v(0)=2\sqrt{w(0)}\,(\sqrt{\eta^2+\mathcal{I}}-\eta)/\mathcal{I}$. Note that this choice does not significantly affect the result as long as $w(0)$ is sufficiently small. The implementation of the numerical solver[23] is done in Python using the packages NumPy 1.21.0[24] and SciPy 1.3.3.[25] The chosen time integrator is an implicit multistep variable-order (1–5) BDF method.

RESULTS AND DISCUSSION

To validate the suggested models, the solutions are compared to the experimental data reported by Heshmati and Piri,[9] where the capillary rise of glycerol, Soltrol 170, and water in vertical glass tubes with constant radii was investigated. These results include both the rise height and the contact angle over time.

Thereafter, the physical basis of the fitted dynamical parameter is elaborated, and further aspects that might have an impact on the experimental and theoretical data are discussed. In particular, the influence of the initial transient regime and of the meniscus shape are considered, as well as possible wetting films and resulting slip in the case of water.

Table 1. Density (ρ), Viscosity (μ), Surface Tension (σ) of the Fluids, and the Tube Radii (R) of the Experiments,[9] and the Static Contact Angle (θ_s) Extracted from Late-Time Data

fluid	ρ (kg/m^3)	μ (Pa s)	σ (N/m)	R (mm)			θ_s (deg)
glycerol	1260	1.011 1	0.063 46	0.250	0.500	1.00	5.63
Soltrol 170	774	0.002 6	0.024 83	0.375	0.500	0.65	9.79
water	997	0.001 1	0.072 8	0.375	0.500	0.65	9.99

https://doi.org/10.1021/acs.langmuir.1c02680
Langmuir 2022, 38, 1680–1688

Table 2. Best-Fit Parameter η ($\pm$ Estimated Standard Deviation) and the Reduced Residual χ^2_ν When Fitting the Upscaled Model to the Experimental Data of the Height (h-fit), the Contact Angle (θ-fit), and Both (both-fit), for the Glycerol Experiments

	h-fit		θ-fit		both-fit	
R (mm)	η	χ^2_ν	η	χ^2_ν	η	χ^2_ν
0.25	0.402 ± 0.010	0.059	0.525 ± 0.008	0.647	0.519 ± 0.006	0.388
0.50	2.356 ± 0.066	0.327	2.151 ± 0.069	2.105	2.183 ± 0.049	1.203
1.00	5.935 ± 0.383	1.226	10.077 ± 0.613	3.985	8.787 ± 0.461	4.053

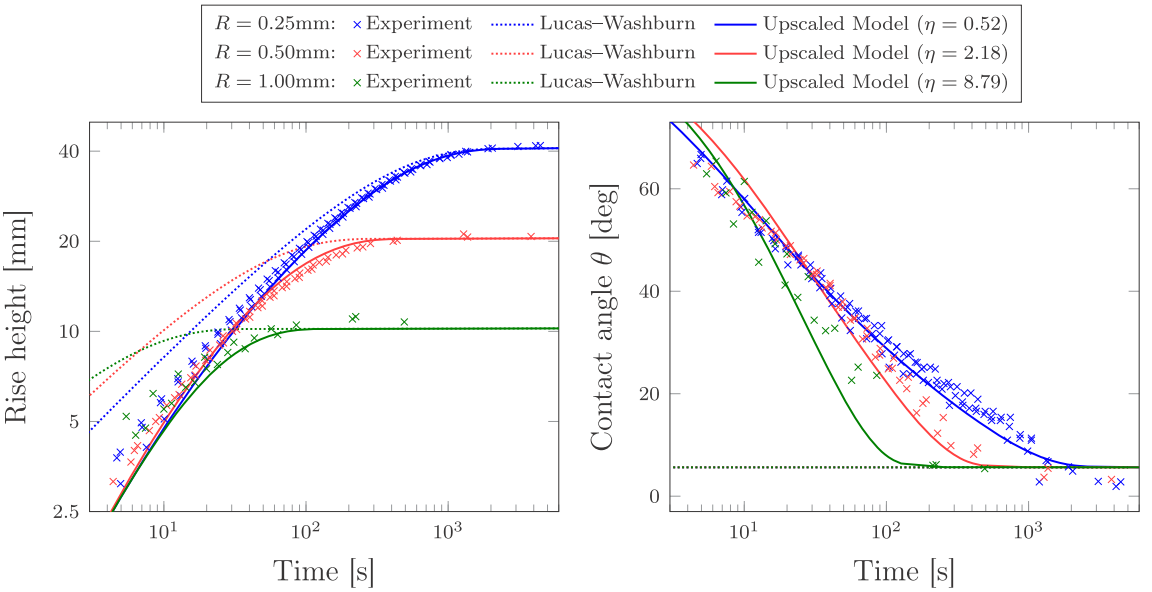

Figure 3. Experimental data for glycerol is matched well by the upscaled model (both-fit). In particular, at early times the representation of the rise is much better than the one for the classical Lucas–Washburn model.

Finally, the uncertainty and limitations of the suggested models and of the fitting are addressed.

Comparison with Experimental Data. The comparison with experimental data is done in three steps. First, the reported physical properties are used for the dimensionless scaling (see also Table 1). Note that the scale ratio ε was below 0.1 in all cases. Second, the late-time data is assumed to be near equilibrium, so that the static contact angle can be extracted from it for each of the three fluids. Note that the resulting static angles (<10°) hardly influence the rise height (<2%), but strongly affect the dynamic contact angle. In the third step, the solutions of the suggested models are matched to the experimental data by fitting the remaining parameters, namely, the dynamic contact-angle parameter (η) and the slip length (λ). For this, for each fluid and each radius separately, a nonlinear least-squares fitting of the rise height (h-fit), of the contact angle (θ-fit), and of both at the same time (both-fit) is performed. Thereby, one can compare the parameter values obtained for the different fits as well as for the different radii to investigate the predictive abilities of the suggested models. The implementation of the procedure[23] is done in Python using the packages pandas 1.3.0[26] and LMFIT 1.0.2.[27]

To illustrate the effect of the dynamic contact-angle model, the classical Lucas–Washburn (LW) solution is also provided. It is obtained from eq. 5 when taking $\eta = 0$ and $\lambda = 0$, using the dimensionless scaling and static contact angle found in the first and second step for comparison.

Glycerol. In the first set of measurements, glycerol was used as the rising fluid. Because of the high viscosity, the inertial effects are negligible ($\mathcal{I} < 1.5 \times 10^{-3}$), so that the solutions to the upscaled model (eq 5) and to the extended one (eq 6) coincide. Therefore, only the results for the upscaled model are presented in Table 2. Note that the simultaneous fitting of the parameters η and λ results in dimensionless slip lengths $\lambda < 10^{-2}$, except for the both-fit at the radius 1.0 mm, which yields $\lambda = 0.026 \pm 0.109$. Hence, slip is negligible and ignored in the subsequent discussion.

The comparison of the experimental data with the fitted upscaled model (eq 3) and the classical Lucas–Washburn model in Figure 3 illustrates the relevance of the dynamic contact angle. While both models match the late-time data when the static contact angle is approached, only the upscaled model with dynamic contact angle agrees with the early time data. In particular, it matches reasonably both the rise height and the contact angle for all three radii. Note that the three fit-types (h, θ, and both) yield different parameters, but the resulting solutions differ only on the scale of the scatter in the experimental data (cf. the Supporting Information). Note that the increase in η with increasing radius is expected, as the dimensional dynamic parameter should be approximately constant. This effect is discussed below for all fluids.

Soltrol. In the second set of measurements, Soltrol 170 was used as the rising fluid. In contrast to the previous case, the extended model differs from the upscaled one ($\mathcal{I} = 1.0$, 4.2, 15.7), but for all radii the best-fit parameters coincide within 1.5 standard deviations (<5% difference), while the residuals are rather lower (−40% to +30% difference, avg. −6%). The minor differences are illustrated in Figure 4, and the results for

https://doi.org/10.1021/acs.langmuir.1c02680
Langmuir 2022, 38, 1680−1688

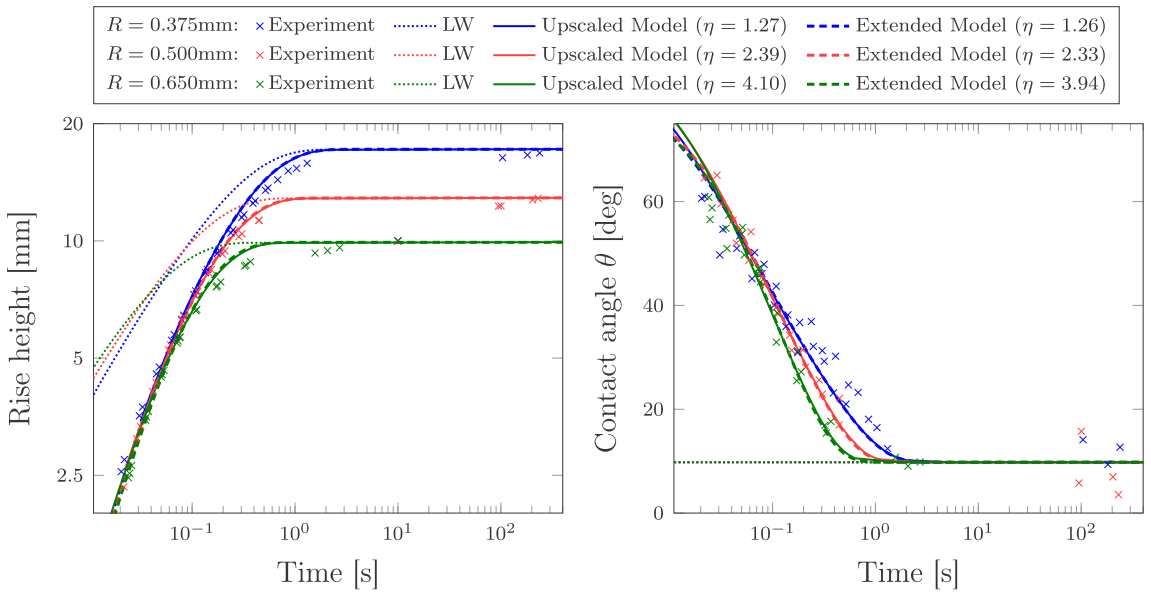

Figure 4. Experimental data for Soltrol 170 is matched almost perfectly by the upscaled model (both-fit), while the classical Lucas−Washburn model (LW) describes only the stationary solution well (after 1 s). For the upscaled and the extended models after fitting, the solutions practically coincide.

Table 3. Best-Fit Parameter η ($\pm$ Estimated Standard Deviation) and the Reduced Residual χ_ν^2 When Fitting the Upscaled Model (top rows) and the Extended Model (bottom rows) to the Experimental Data of the Height (h-fit), the Contact Angle (θ-fit), and Both (both-fit), for the Soltrol 170 Experiments

	h-fit		θ-fit		both-fit	
R (mm)	η	χ_ν^2	η	χ_ν^2	η	χ_ν^2
0.375	1.464 ± 0.067	0.313	1.250 ± 0.058	2.153	1.273 ± 0.042	1.232
0.500	2.521 ± 0.080	0.196	2.358 ± 0.081	1.042	2.386 ± 0.056	0.603
0.650	4.588 ± 0.162	0.414	3.963 ± 0.143	1.370	4.098 ± 0.108	0.951
0.375	1.437 ± 0.005	0.340	1.241 ± 0.027	2.239	1.261 ± 0.044	1.275
0.500	2.430 ± 0.075	0.207	2.309 ± 0.062	0.623	2.330 ± 0.045	0.403
0.650	4.370 ± 0.016	0.537	3.830 ± 0.024	1.183	3.944 ± 0.122	0.899

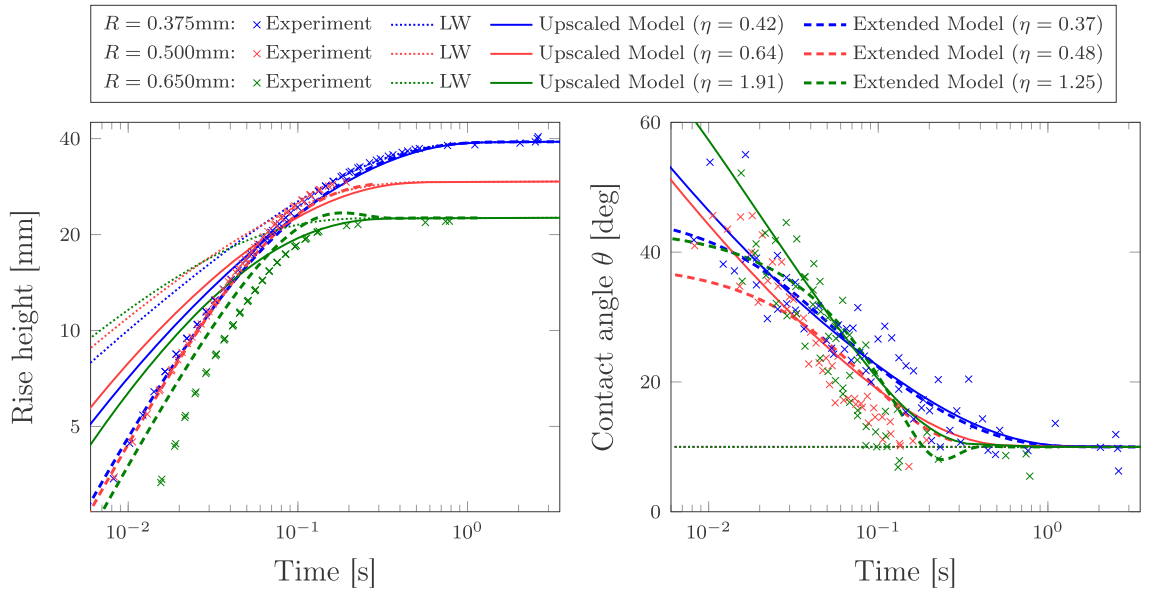

Figure 5. Experimental data for water is matched well by the extended model (both-fit), while the upscaled model (both-fit) matches only the contact angle and late-time data (after ∼0.05 s). The classical Lucas−Washburn (LW) model describes only the stationary solution well (after 0.1 s).

https://doi.org/10.1021/acs.langmuir.1c02680
Langmuir 2022, 38, 1680−1688

Table 4. Best-Fit Parameter η ($\pm$ Standard Deviation) and the Reduced Residual χ_ν^2 When Fitting the Extended Model (without slip) to the Experimental Data of the Height (h-fit), the Contact Angle (θ-fit), and Both (both-fit) for the Water Experiments

	h-fit		θ-fit		both-fit	
R (mm)	η	χ_ν^2	η	χ_ν^2	η	χ_ν^2
0.375	0.162 ± 0.005	0.058	0.377 ± 0.017	2.054	0.367 ± 0.013	1.143
0.500	0.111 ± 0.020	0.153	0.498 ± 0.037	3.914	0.476 ± 0.026	2.249
0.650	2.849 ± 0.064	0.234	1.052 ± 0.079	4.595	1.248 ± 0.079	4.203

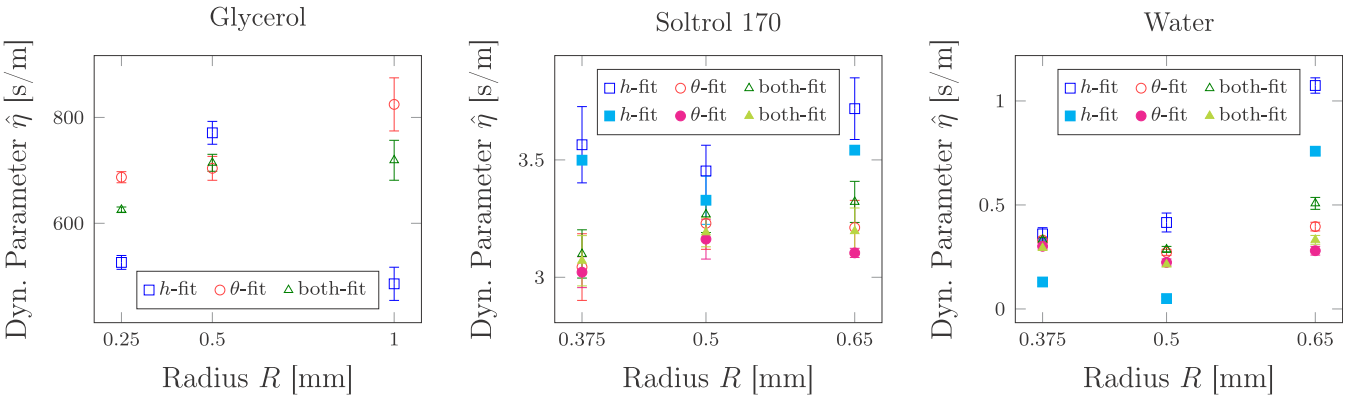

Figure 6. Dimensional dynamic parameter $\hat{\eta}$ of the models (empty, upscaled; filled, extended) fitted to the experimental data of the height (h-fit), the contact angle (θ-fit), and both (both-fit). Observe that these parameters vary significantly from one fluid to another but appear to not depend on the tube radius.

both models are reported in Table 3. Note that the fit of the dimensionless slip length yields $\lambda < 10^{-6}$ in all cases, which is again negligible and thus ignored.

For Soltrol, the fitted upscaled model (eq 5) matches the experimental data almost perfectly, while the classical Lucas–Washburn model predicts only the stationary solution well (see Figure 4). In particular, the upscaled model with dynamic contact angle agrees with the data of both the rise height and the contact angle for all three radii and at all times. For more details, see also the Supporting Information. The fit of the extended model coincides with that of the upscaled model. Only at very early times (until 0.05 s) does the extended model predict a slightly lower contact angle. These early time dynamics are especially relevant for larger radii and less viscous fluids like water, as shown and discussed below.

Water. In the last set of measurements, distilled water was used as the rising fluid. In contrast to the previous cases, the extended model differs significantly from the upscaled one ($\mathcal{I} = 4.1, 17, 64$) (see Figure 5). The upscaled model (both-fit) matches only the contact angle and late-time height (after ~0.05 s). The experimental data is much better represented by the extended model; hence, only these results are reported in Table 4. More details and the results of the upscaled model can be found in the Supporting Information. Note that the fit of the dimensionless slip length was inconsistent ($\lambda < 0.15$) with generally large standard deviation. For the θ-fits, the slip was negligible ($\lambda < 10^{-9}$), while the other fits suggest the occurrence of an effective slip, which might be due to prewetting films, as discussed below.

For water, the fitted extended model matches reasonably the experimental data, although the rise height is slightly overpredicted (+10%) for the radius $R = 0.65$ mm (see Figure 5). In particular, note that the model predicts an overshoot (between 0.2 and 0.4 s). The experimental data does not show this behavior. Instead, the rise seems delayed compared to the other experiments (3.4 vs 6.5–7.4 mm at time 0.016 s).

Dynamic Parameter as Physical Property. The dynamic parameter η obtained by fitting can be interpreted as a physical property of the fluid system. For this, dimensional quantities are marked with a hat. Although the different fitting criteria, namely, the height, the contact angle, or both, provide optimal parameters with significant variation, the dynamic parameter $\hat{\eta}$ [s/m] (scaling $\mu/(\rho g R^2)$) seems to be independent of the tube radius (see Figure 6). This agrees with the results reported by Hamraoui et al.,[12,21] where the Lucas–Washburn equation with dynamic contact angle was compared with experiments of ethanol, water, and silicon oil in glass tubes, and those obtained by Martic et al.[10] for molecular dynamics simulations. Further experimental data considering a larger range of radii and hence velocities are necessary to confirm this hypothesis.

Note that the closely related linearized molecular-kinetic theory[10−12,20−22] yields the dynamic contact-angle model

$$\cos(\theta_s) - \cos(\theta) = \xi \hat{v}$$

where $\hat{v}$ denotes the contact line velocity. Here, the intrinsic friction coefficient ξ (s/m) is proportional to the ratio μ/σ of the viscosity to the fluid–air surface tension. Therefore, one expects an almost constant ratio $\hat{\eta}\sigma/\mu$ for all fluids, which is also found for the fitted parameter $\hat{\eta}$, because the ratio is ca. 30–70 for glycerol, ca. 25–35 for Soltrol 170, and ca. 5–50 for water. Finally, Martic et al.[11] demonstrated that neglecting the dynamic parameter can lead to significant underestimation of the effective pore radius in porous media.

Influence of the Initial Transient Regime. At the start of the experiment, the tube touches the surface of the fluid in the reservoir. This topological change initiates the rise and the meniscus shape, which are hence strongly affected by the (touch) speed and the exact (nanometric) surface of the tube tip. In the suggested models, this initial transient regime is

https://doi.org/10.1021/acs.langmuir.1c02680
Langmuir 2022, 38, 1680−1688

neglected, and a stable Hagen−Poiseuille flow profile and a spherical meniscus are assumed to form quasi-instantaneously. To understand the details better, accurate microscale analysis and simulations in the initial stage are necessary. For microgravity experiments, Stange et al.[28] found three successive phases: a quadratic dependence of the meniscus height on time ($h \sim t^2$); followed by a linear increase ($h \sim t$); and finally, the Lucas−Washburn behavior ($h^2 \sim t$).

However, the fitting results suggest that the initial transient regime is indeed negligible here, especially for glycerol and Soltrol 170 (cf. the above comparison), for which one could even neglect inertia. Nevertheless, for large radii, as well as less viscous fluids, such as water, these effects might be significant. In particular, the water experiment with largest radius (R = 0.65 mm) shows deviations from an initially linear height−time relation (see Figure 5 and the Supporting Information). Additionally, for such regimes, the proper choice of the (numerical) initial conditions for the extended model eq 6 might be important. Here, they are based on asymptotic analysis to approach $t = 0$ and a sufficiently small numerical regularization with negligible impact on the solution. Further investigation can lead to conditions (or extensions) that include the transient effect.

Meniscus Shape. The meniscus shape is assumed spherical for the experimental measurement of the contact angle, as well as for the discussed models. However, this shape might be deformed because of the influence of the inertia and gravity. For glycerol and Soltrol 170, the agreement of the experimental contact-angle data and the fitted upscaled model gives confidence that these effects can be neglected. For water, the experimental contact angle data has a rather large scatter, and the differences between experiments and fitted models are higher (cf. Figure 5 and the Supporting Information). For experiments with water in glass tubes of lower radius (R = 0.15 mm and R = 0.2 mm), Xue et al.[8] reported that the rise velocity is too high to have a spherical meniscus shape. Therefore, the obtained results for the contact angle of water should be treated with caution.

Wetting Films and Slip. For glycerol and Soltrol 170, Heshmati and Piri[9] vacuum-dried the tubes immediately before the experiments, so that no prewetting films were present. The model fitting resulted accordingly in negligible slip lengths, $\lambda < 10^{-2}$, which translates into a dimensional slip length below 1 μm. In contrast, the tubes for the experiments with water were only partially dried using a paper filter, to avoid contamination affecting the contact angle and the equilibrium rise.[9] Hence, heterogeneous prewetting films of water could possibly be present in the tubes. This can influence the contact angle and the meniscus shape and induces difficulties for the measurements and the modeling, so that a direct comparison becomes more involved.

Additionally, the presence of wetting films would reduce the dissipation from the formation of water−glass interfacial area. Hence, the water rises faster, which corresponds to an effective slip in the presented models. In the fitting of the extended model using the height data (h-fit and both-fit), indeed, a relevant slip length up to 0.15 (dimension of about 0.1 mm, cf. the Supporting Information) was observed. However, the dynamic coefficient (η) and the slip length (λ) are strongly correlated, such that the slip length in the model is difficult to relate to the physical behavior.

Furthermore, note that negative effective slip was observed for nanometric pores.[29] There, the effective slip length depends on the wettability and the viscosity, which considerably differs for confined water near walls and for bulk water. Here, however, the fitting did not allow for negative slip lengths, because these effects were found to be relevant only for radii on the nanometer scale.[29]

Uncertainty and Limitations of the Suggested Models and of the Fitting. Because the suggested models are derived in leading order for $\varepsilon \ll 1$, errors in the order of ε are expected (here $\varepsilon < 0.01$). Furthermore, a linearized dynamic contact-angle model is chosen here for simplicity. A higher accuracy can be obtained using a more sophisticated contact-angle model, which, itself, needs further investigation and validation.[14,20] Additionally, a Hagen−Poiseuille flow is assumed for the extended model. Deviations due to inertial effects are ignored but might affect the inertial coefficient $\mathcal{I}$. This could explain the overshoot observed for the extended model in the case of water with tube radius R = 0.65 mm (cf. Figure 5), which is not present in the experiment.

Furthermore, the static contact angle is highly sensitive to the used materials. In contrast to the total wetting ($\theta = 0°$) used by Heshmati and Piri,[9] the values extracted from the experiments range between 5° and 10°. Note that, for water−air−glass systems, even a static contact angle of 20−30° is reported by Li et al.[30] Although this has only a minor influence on the rise height, it affects the fitting for the dynamic contact angle.

CONCLUSIONS

The upscaled model of capillary-driven flow in circular cylindrical tubes extends the classical Lucas−Washburn theory by incorporating a dynamic contact angle. Using a simple relation between the contact angle and the velocity of the moving contact line, an analytical expression for the capillary rise over time was derived. Based on empirical arguments, the mathematical model was extended to account for inertial effects.

To validate the models, the solutions were compared to the experimental data observed by Heshmati and Piri.[9] In contrast to the Lucas−Washburn model, the models with dynamic contact angle do match the experimental data, both the rise height and the contact angle, even at early times. The fitting procedure requires only one parameter for the dynamic contact angle. In particular, the findings suggest that this parameter depends only on the physical properties of the involved fluids (and of the tube) but is independent of geometrical features, such as the radius of the tube. Therefore, the presented models can be used to predict capillary-driven flow in tubular systems upon knowledge of the underlying dynamic contact-angle relation.

In future work, this approach will be used to construct dynamic pore-network models, to study the resulting dynamic core-scale effects, and to derive upscaled models valid on a possibly larger scale.

ASSOCIATED CONTENT

Supporting Information

The Supporting Information is available free of charge at https://pubs.acs.org/doi/10.1021/acs.langmuir.1c02680.

Details of the upscaling procedure and of the comparison between model solutions and experimental data (PDF)

https://doi.org/10.1021/acs.langmuir.1c02680
Langmuir 2022, 38, 1680−1688

AUTHOR INFORMATION

Corresponding Author

Stephan B. Lunowa − *Computational Mathematics, UHasselt − Hasselt University, 3590 Diepenbeek, Belgium;* orcid.org/0000-0002-5214-7245; Email: stephan.lunowa@uhasselt.be

Authors

Arjen Mascini − *Pore-Scale Processes in Geomaterials Research Group (PProGRess), Department of Geology, Ghent University, 9000 Ghent, Belgium*

Carina Bringedal − *Institute for Modelling Hydraulic and Environmental Systems, University of Stuttgart, 70569 Stuttgart, Germany*

Tom Bultreys − *Pore-Scale Processes in Geomaterials Research Group (PProGRess), Department of Geology, Ghent University, 9000 Ghent, Belgium*

Veerle Cnudde − *Pore-Scale Processes in Geomaterials Research Group (PProGRess), Department of Geology, Ghent University, 9000 Ghent, Belgium; Environmental Hydrogeology Group, Department of Earth Sciences, Utrecht University, 3584CB Utrecht, The Netherlands*

Iuliu Sorin Pop − *Computational Mathematics, UHasselt − Hasselt University, 3590 Diepenbeek, Belgium*

Complete contact information is available at: https://pubs.acs.org/10.1021/acs.langmuir.1c02680

Author Contributions

CRediT author statement: S.B.L.: Conceptualization, Data curation, Formal analysis, Investigation, Methodology, Software, Validation, Visualization, Writing - original draft. A.M.: Conceptualization, Methodology, Investigation, Validation, Writing - review and editing. C.B.: Conceptualization, Methodology, Writing - review and editing. T.B.: Conceptualization, Funding acquisition, Writing - review and editing. V.C.: Conceptualization, Funding acquisition, Writing - review and editing. I.S.P.: Conceptualization, Funding acquisition, Methodology, Writing - review and editing.

Notes

The authors declare no competing financial interest.

The data that support the findings of this study was generated using the source code[23] which is openly available at https://github.com/s-lunowa/dynamic-capillary-rise.

ACKNOWLEDGMENTS

The authors are grateful to Mohammad Heshmati and Mohammad Piri for providing their experimental data. The authors thank the Deutsche Forschungsgemeinschaft (DFG, German Research Foundation) for supporting this work by funding the Collaborative Research Center on Interface-Driven Multi-Field Processes in Porous Media (SFB 1313, grant number 327154368) and by funding EXC 2075-390740016 under Germany's Excellence Strategy. We acknowledge support by the Stuttgart Centre for Simulation Science (SimTech). This work was supported by Hasselt University (project number BOF17NI01) and the Research Foundation Flanders (FWO) [grant numbers G051418N, G0G1316N, and 12X0919N]; Tom Bultreys is a postdoctoral fellow of the Research Foundation Flanders.

REFERENCES

(1) Lucas, R. Über das Zeitgesetz des kapillaren Aufstiegs von Flüssigkeiten. *Kolloid-Z.* **1918**, *23*, 15−22.

(2) Washburn, E. W. The dynamics of capillary flow. *Phys. Rev.* **1921**, *17*, 273−283.

(3) Rideal, E. K. On the flow of liquids under capillary pressure. *Philos. Mag.* **1922**, *44*, 1152−1159.

(4) Bosanquet, C. H. On the flow of liquids into capillary tubes. *Philos. Mag.* **1923**, *45*, 525−531.

(5) Cai, J.; Jin, T.; Kou, J.; Zou, S.; Xiao, J.; Meng, Q. Lucas−Washburn equation-based modeling of capillary-driven flow in porous systems. *Langmuir* **2021**, *37*, 1623−1636.

(6) Fries, N.; Dreyer, M. An analytic solution of capillary rise restrained by gravity. *J. Colloid Interface Sci.* **2008**, *320*, 259−263.

(7) Levine, S.; Lowndes, J.; Watson, E. J.; Neale, G. A theory of capillary rise of a liquid in a vertical cylindrical tube and in a parallel-plate channel: Washburn equation modified to account for the meniscus with slippage at the contact line. *J. Colloid Interface Sci.* **1980**, *73*, 136−151.

(8) Xue, H. T.; Fang, Z. N.; Yang, Y.; Huang, J. P.; Zhou, L. W. Contact angle determined by spontaneous dynamic capillary rises with hydrostatic effects: Experiment and theory. *Chem. Phys. Lett.* **2006**, *432*, 326−330.

(9) Heshmati, M.; Piri, M. Experimental investigation of dynamic contact angle and capillary rise in tubes with circular and noncircular cross sections. *Langmuir* **2014**, *30*, 14151−14162.

(10) Martic, G.; Gentner, F.; Seveno, D.; Coulon, D.; De Coninck, J.; Blake, T. D. A molecular dynamics simulation of capillary imbibition. *Langmuir* **2002**, *18*, 7971−7976.

(11) Martic, G.; De Coninck, J.; Blake, T. D. Influence of the dynamic contact angle on the characterization of porous media. *J. Colloid Interface Sci.* **2003**, *263*, 213−216.

(12) Hamraoui, A.; Nylander, T. Analytical approach for the Lucas−Washburn equation. *J. Colloid Interface Sci.* **2002**, *250*, 415−421.

(13) Chebbi, R. Dynamics of liquid penetration into capillary tubes. *J. Colloid Interface Sci.* **2007**, *315*, 255−260.

(14) Popescu, M. N.; Ralston, J.; Sedev, R. Capillary rise with velocity-dependent dynamic contact angle. *Langmuir* **2008**, *24*, 12710−12716.

(15) Quéré, D. Inertial capillarity. *Europhys. Lett.* **1997**, *39*, 533−538.

(16) Xiao, Y.; Yang, F.; Pitchumani, R. A generalized analysis of capillary flows in channels. *J. Colloid Interface Sci.* **2006**, *298*, 880−888.

(17) Zhmud, B. V.; Tiberg, F.; Hallstensson, K. Dynamics of capillary rise. *J. Colloid Interface Sci.* **2000**, *228*, 263−269.

(18) Fries, N.; Dreyer, M. The transition from inertial to viscous flow in capillary rise. *J. Colloid Interface Sci.* **2008**, *327*, 125−128.

(19) Lunowa, S. B.; Bringedal, C.; Pop, I. S. On an averaged model for immiscible two-phase flow with surface tension and dynamic contact angle in a thin strip. *Stud. Appl. Math.* **2021**, *147*, 84−126.

(20) Blake, T. D. The physics of moving wetting lines. *J. Colloid Interface Sci.* **2006**, *299*, 1−13.

(21) Hamraoui, A.; Thuresson, K.; Nylander, T.; Yaminsky, V. Can a dynamic contact angle be understood in terms of a friction coefficient? *J. Colloid Interface Sci.* **2000**, *226*, 199−204.

(22) Ramakrishnan, T.; Wu, P.; Zhang, H.; Wasan, D. T. Dynamics in closed and open capillaries. *J. Fluid Mech.* **2019**, *872*, 5−38.

(23) Lunowa, S. B. Software for fitting the upscaled and extended model of capillary rise to experimental data. 2021; https://github.com/s-lunowa/dynamic-capillary-rise.

(24) Harris, C. R.; Millman, K. J.; van der Walt, S. J.; Gommers, R.; Virtanen, P.; Cournapeau, D.; Wieser, E.; Taylor, J.; Berg, S.; Smith, N. J.; Kern, R.; Picus, M.; Hoyer, S.; van Kerkwijk, M. H.; Brett, M.; Haldane, A.; del Río, J. F.; Wiebe, M.; Peterson, P.; Gérard-Marchant, P.; Sheppard, K.; Reddy, T.; Weckesser, W.; Abbasi, H.; Gohlke, C.; Oliphant, T. E. Array programming with NumPy. *Nature* **2020**, *585*, 357−362.

(25) Virtanen, P.; Gommers, R.; Oliphant, T. E.; Haberland, M.; Reddy, T.; Cournapeau, D.; Burovski, E.; Peterson, P.; Weckesser, W.; Bright, J.; van der Walt, S. J.; Brett, M.; Wilson, J.; Millman, K. J.; Mayorov, N.; Nelson, A. R. J.; Jones, E.; Kern, R.; Larson, E.; Carey, C. J.; Polat, İ.; Feng, Y.; Moore, E. W.; VanderPlas, J.; Laxalde, D.; Perktold, J.; Cimrman, R.; Henriksen, I.; Quintero, E. A.; Harris, C. R.; Archibald, A. M.; Ribeiro, A. H.; Pedregosa, F.; van Mulbregt, P.; Vijaykumar, A.; Bardelli, A. P.; Rothberg, A.; Hilboll, A.; Kloeckner, A.; Scopatz, A.; Lee, A.; Rokem, A.; Woods, C. N.; Fulton, C.; Masson, C.; Häggström, C.; Fitzgerald, C.; Nicholson, D. A.; Hagen, D. R.; Pasechnik, D. V.; Olivetti, E.; Martin, E.; Wieser, E.; Silva, F.; Lenders, F.; Wilhelm, F.; Young, G.; Price, G. A.; Ingold, G.-L.; Allen, G. E.; Lee, G. R.; Audren, H.; Probst, I.; Dietrich, J. P.; Silterra, J.; Webber, J. T.; Slavič, J.; Nothman, J.; Buchner, J.; Kulick, J.; Schönberger, J. L.; de Miranda Cardoso, J. V.; Reimer, J.; Harrington, J.; Rodríguez, J. L. C.; Nunez-Iglesias, J.; Kuczynski, J.; Tritz, K.; Thoma, M.; Newville, M.; Kümmerer, M.; Bolingbroke, M.; Tartre, M.; Pak, M.; Smith, N. J.; Nowaczyk, N.; Shebanov, N.; Pavlyk, O.; Brodtkorb, P. A.; Lee, P.; McGibbon, R. T.; Feldbauer, R.; Lewis, S.; Tygier, S.; Sievert, S.; Vigna, S.; Peterson, S.; More, S.; Pudlik, T.; Oshima, T.; Pingel, T. J.; Robitaille, T. P.; Spura, T.; Jones, T. R.; Cera, T.; Leslie, T.; Zito, T.; Krauss, T.; Upadhyay, U.; Halchenko, Y. O.; Vázquez-Baeza, Y. SciPy 1.0 Contributors, SciPy 1.0: Fundamental algorithms for scientific computing in Python. *Nat. Methods* **2020**, *17*, 261−272.

(26) Reback, J.; jbrockmendel; McKinney, W.; Van den Bossche, J.; Augspurger, T.; Cloud, P.; Hawkins, S.; gfyoung; Sinhrks; Roeschke, M.; Klein, A.; Petersen, T.; Tratner, J.; She, C.; Ayd, W.; Hoefler, P.; Naveh, S.; Garcia, M.; Schendel, J.; Hayden, A.; Saxton, D.; Gorelli, M. E.; Shadrach, R.; Jancauskas, V.; McMaster, A.; Li, F.; Battiston, P.; Seabold, S.; attack68; Dong, K. *pandas-dev/pandaspandas-dev/pandas: Pandas 1.3.0*. 2021; DOI: 10.5281/zenodo.5060318.

(27) Newville, M.; Otten, R.; Nelson, A.; Ingargiola, A.; Stensitzki, T.; Allan, D.; Fox, A.; Carter, F.; Michał; Pustakhod, D.; lneuhaus; Weigand, S.; Osborn, R.; Glenn; Deil, C.; Mark; Hansen, A. L. R.; Pasquevich, G.; Foks, L.; Zobrist, N.; Frost, O.; Beelen, A.; Stuermer; kwertyops; Polloreno, A.; Caldwell, S.; Almarza, A.; Persaud, A.; Gamari, B.; Maier, B. F. *lmfit/lmfit-py 1.0.2*. 2021; DOI: 10.5281/zenodo.4516651.

(28) Stange, M.; Dreyer, M. E.; Rath, H. J. Capillary driven flow in circular cylindrical tubes. *Phys. Fluids* **2003**, *15*, 2587−2601.

(29) Zeng, F.; Zhang, Q.; Guo, J.; Meng, Y.; Shao, X.; Zheng, Y. Capillary imbibition of confined water in nanopores. *Capillarity* **2020**, *3*, 8−15.

(30) Li, X.; Fan, X.; Brandani, S. Difference in pore contact angle and the contact angle measured on a flat surface and in an open space. *Chem. Eng. Sci.* **2014**, *117*, 137−145.

https://doi.org/10.1021/acs.langmuir.1c02680
Langmuir 2022, 38, 1680−1688